Preparation of composite adsorbents of activated carbon supported MgO/MnO_2 and adsorption of Rhodamine B

Xiangfeng Yue, Jianhai Zhao, Huanhuan Shi, Yongzhi Chi and Muhammad Salam

ABSTRACT

Activated carbon (AC) was modified by MgO and MnO_2 through an impregnation-precipitation-calcination procedure. The batch experiments of adsorption of Rhodamine B (RB) by a modified adsorption material, an MgO-MnO_2-AC composite, were carried out and the characteristics of the composite adsorbent were evaluated. The results showed that manganese/magnesium loading changed the surface area, pore volume and increased the number of active adsorption sites of AC. The highest Brunauer-Emmett-Teller (BET) surface area (1,036.18 $m^2 \cdot g^{-1}$) was obtained for MgO-MnO_2-AC compared with AC. The content of AC loaded with magnesium and manganese was 34.24 and 5.51 $mg \cdot g^{-1}$ respectively. The adsorption of RB on MgO-MnO_2-AC was significantly improved. The maximum adsorption capacity of RB on MgO-MnO_2-AC was 16.19 $mg \cdot g^{-1}$ at 25 °C under the RB concentration of 50 $mg \cdot L^{-1}$. The adsorption of RB by AC and MgO-MnO_2-AC increased with the initial concentration of RB. The adsorption of RB increased first and then decreased when pH was between 3 and 11. The results indicated that the pseudo-second-order kinetic equation and Langmuir equation can be used to describe the adsorption of RB on MgO-MnO_2-AC.

Key words | activated carbon, adsorption, magnesium oxide, manganese dioxide, Rhodamine B

Xiangfeng Yue
Jianhai Zhao (corresponding author)
Huanhuan Shi
Yongzhi Chi
Tianjin Key Laboratory of Aquatic Science and Technology,
School of Environmental and Municipal Engineering, Tianjin Chengjian University,
Tianjin 300384,
China
E-mail: *jhzhao@tcu.edu.cn*

Muhammad Salam
School of Ecology and Environmental Science,
Chongqing University,
Chongqing 400044,
China

HIGHLIGHTS

- Composite adsorbents of activated carbon supported MgO/MnO_2 were prepared.
- Characteristics of MgO-MnO_2-AC were analyzed.
- MgO-MnO_2-AC had high adsorption capacity for Rhodamine B.
- Adsorption data agreed well with a pseudo-second-order kinetic model.
- Langmuir model was better for fitting the adsorption equilibrium isotherm.

GRAPHICAL ABSTRACT

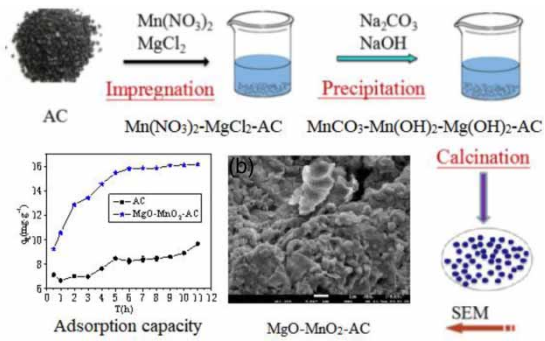

doi: 10.2166/wst.2020.172

INTRODUCTION

Dye wastewater from textiles and other industrial areas is difficult to remove due to its different chemical structure and large yield. Dyes in water have the characteristics of mutagenicity, toxicity, sensitization, carcinogenicity, non-degradation, good stability to light and oxidants, and resistance to aerobic digestion, and also have important effects on ecological systems and human health (Cheng *et al.* 2016; Gupta *et al.* 2016; Maeda *et al.* 2018). Rhodamine B (RB) is a basic dye molecule that is widely used in textile printing, dyeing, etc. (Ahmed *et al.* 2018; Qi *et al.* 2019; Song *et al.* 2019). Common methods for removing dyes in water include coagulation (Wang *et al.* 2016), electrolysis (Li *et al.* 2015), biodegradation (Liu *et al.* 2016a, 2016b), advanced oxidation (Xu *et al.* 2018) and adsorption (Qi *et al.* 2019), etc. As an adsorbent with a large specific surface area, activated carbon (AC) is often used to adsorb dye wastewater (Zhang *et al.* 2018). However, the adsorption capacity of AC to dye is still relatively small. In order to increase the adsorption capacity of activated carbon, many researchers have focused on research into activated carbon surface modification which can improve its surface characteristics to obtain better adsorption capacity.

Metal ion modification is a simple and effective method to improve the adsorption capacity of AC (Liu *et al.* 2017). The removal capacity for methylene blue of AC increased 17.12% by impregnating $Fe(NO_3)_3$ onto AC (Cheng *et al.* 2016). Granular activated carbon supported magnesium hydroxide had a better adsorption capacity to cadmium (II) than untreated granular activated carbon (Wang *et al.* 2016). Common modification methods include sol-gel (Ciesielczyk *et al.* 2017), impregnation (Rojasmayorga *et al.* 2015), calcinations (Jin *et al.* 2018), microwave (Liu *et al.* 2016a, 2016b) and co-precipitation (Wang *et al.* 2016). Calcining can effectively change the pore structure, dispersion and surface properties of the material (Yuan *et al.* 2013). Magnesium oxide and manganese dioxide are good catalysts and adsorbents for environmental protection (Shaabani *et al.* 2015; Ahmed *et al.* 2018; Zhang *et al.* 2019). A granular activated carbon microporous adsorbent coated with magnesium oxide was used to remove benzene from the air (Rashidi *et al.* 2019). Chemically modified activated carbon loaded with manganese dioxide nanoparticles enhanced the adsorption capacity of activated carbon for Li^+ adsorption from aqueous media (Kamran *et al.* 2019). Although the use of manganese/magnesium modified adsorbents has been reported widely, there is little information about the effect of Mn/Mg on the adsorption properties of active carbons.

The main objectives of the presented work focus on loading both magnesium oxide and manganese dioxide onto AC by impregnation-coprecipitation-calcination. Batch adsorption tests were used to study the adsorption mechanism. The adsorption characteristics of RB on original and modified activated carbon were analyzed by scanning electron microscopy (SEM), Brunauer-Emmett-Teller (BET) and X-ray diffraction (XRD) analysis. Adsorption isotherms and adsorption kinetics were discussed.

EXPERIMENTAL METHODS

Materials and reagents

Activated carbon (AC) was purchased from an activated carbon factory in Henan. It was screened into diameters of 1 to 3 mm. Rhodamine B was used as an adsorbate compound and was received from Tianjin Dongya Company. The molecular structure and molecular formula of RB are presented in Table 1. Stock solutions of $Mn(NO_3)_2$, $MgCl_2$ and Na_2CO_3 were prepared by dissolving reagent-grade metal salts, $Mn(NO_3)_2$ (Tianjin Guangfu), $MgCl_2{\cdot}6H_2O$ (Tianjin Chemical Reagent Co.) and Na_2CO_3 (Tianjin Wind Ship) in distilled water, respectively.

Preparation of modified activated carbon

AC was washed several times with deionized water to remove surface dust and impurities, then dried at 90 °C for 3 h. A total of 10 g AC was mixed with 150 ml of a 0.1 $mol{\cdot}L^{-1}$ $Mn(NO_3)_2$ and 0.5 $mol{\cdot}L^{-1}$ $MgCl_2$ solution using a 250 ml conical flask, and the mixture was agitated at 25 °C and 180 rpm for 2 h. After filtering, washing and drying, $MgCl_2$-$Mn(NO_3)_2$-AC compounds are obtained. Then, the compounds were reacted with 100 ml of a 0.5 $mol{\cdot}L^{-1}$ Na_2CO_3 and 0.5 $mol{\cdot}L^{-1}$ NaOH solution for some time, then filtered, washed and dried to obtain

Table 1 | Dye characteristics

Name	Molecular formula	Molecular structure
Rhodamine B	$C_{28}H_{31}ClN_2O_3$	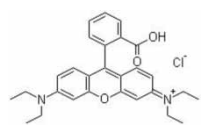

a sample $Mg(OH)_2$-$MnCO_3$-AC compound. The sample was calcined in a furnace at 360 °C for 2.5 h, and named MgO-MnO_2-AC.

Structural characterization

The surface micromorphology of MgO-MnO_2-AC composite materials was observed by SEM using a JSM-7800F scanning electron microscope (Quanta 200, FEI, Czech Republic). Element contents were observed by ICP-MAS (inductively coupled plasma mass spectrometry, Agilent 7000E, USA). The N_2 adsorption-desorption isotherms were recorded using a nitrogen gas adsorption analyzer (ASAP 2020, Micromeritics, USA). The specific surface area of the sample was determined by the BET method. The X-ray diffractometer (Ultima IV, Rigaku Corporation, Japan) was used on the crystal form of AC and MgO-MnO_2-AC.

Batch adsorption experiments

Batch adsorption experiments were conducted in 250 ml conical flasks with different initial adsorbate concentrations, pH, temperatures, and addition of adsorbent. AC and MgO-MnO_2-AC modified materials were used as adsorbents for RB dye adsorption. The flasks were placed in a thermostatic oscillator at a speed of 200 rpm and reacted for 3 h without light. Then, the supernatant was filtered with a 0.45 μm filter membrane, the filtrates' concentration of RB was analyzed by a UV-Vis spectrophotometer (UV2550, Shimadzu, Japan).

The adsorption capability and removal efficiency were calculated using the following Equations (1) and (2)

$$q_e = \frac{(C_0 - C_e)V}{m} \quad (1)$$

$$\mathrm{E} = \frac{C_0 - C_e}{C_0} \times 100\% \quad (2)$$

where q_e (mg·g^{-1}) is the experimental adsorption capability, E (%) is the removal efficiency, C_0 (mg·L^{-1}) and C_e (mg·L^{-1}) are the initial and equilibrated RB concentration, respectively, V (mL) is the volume of the solution and m (g) is the mass of the adsorbent.

Adsorption kinetics

The adsorption kinetics study of MgO-MnO_2-AC was performed by adding 0.3 g of sample and 100 ml of varying RB solutions (10, 50, 100 mg·L^{-1}) to 250 ml conical flasks with stoppers. Then, all conical flasks were shaken at a constant agitation speed (200 rpm) at 25 °C. Samples were obtained at 1–11 h, respectively. The supernatant solution was filtered with a 0.45 μm filter membrane and the absorbance was measured.

Adsorption isotherms

For the adsorption isothermal study, 0.3 g MgO-MnO_2-AC was mixed with 100 ml varying initial RB concentrations (10–60 mg·L^{-1}) using 250 ml conical flasks with stoppers. The flasks were shaken in a thermostatic oscillator at a constant agitation speed (220 rpm) for 10 h at pH 7.6. Reaction temperatures were set at 25 °C, 35 °C, and 45 °C. The supernatant solution was filtered with a 0.45 μm filter membrane and the absorbance measured.

RESULTS AND DISCUSSION

Characteristics of MgO-MnO_2-AC

The structures and properties of the original and modified activated carbon are presented in Table 2. The surface area and total pore volume of AC increased to some extent after modification by MgO and MnO_2, which can provide more active sites for RB. This indicates that the formation of MgO and MnO_2 increased the specific surface area and pore volume of the original activated carbon. The decrease in average pore diameter is due to the formation of load on the pore wall (Riverautrilla *et al.* 2017). Pore size distribution (PSD) is one of the important properties of AC, which determines the contact distribution of molecules in the whole pore volume. As can be seen from Figure 1(a), MgO-MnO_2-AC contains a large number of micropores and a part of mesoporous pores, and the number of micropores and mesoporous holes is more than the original AC. This may be due to the removal of impurities caused by calcining and the formation of new structures on the surface and inside the MgO-MnO_2-AC.

Table 2 | Physical parameters of original and modified activated carbon

Materials	BET $m^2 \cdot g^{-1}$	V_t ($cm^3 \cdot g^{-1}$)	D_p (nm)
AC	707.55	0.13	1.41
MgO-MnO_2-AC	1036.18	0.48	1.23

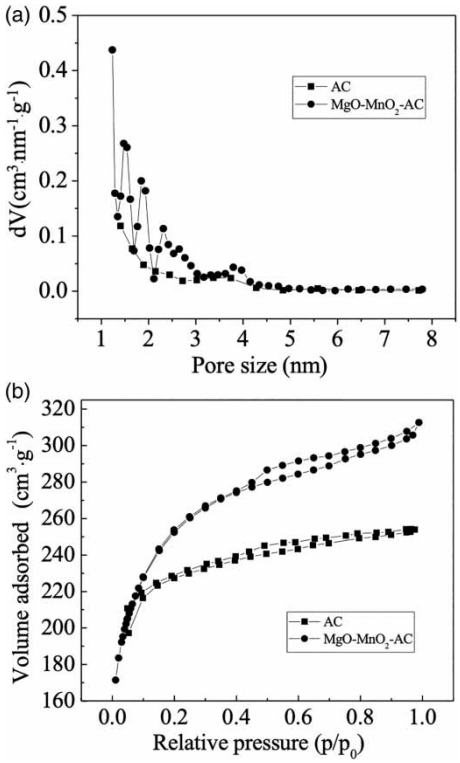

Figure 1 | Characteristics of adsorbents (a: Pore size distributions, b: Nitrogen adsorption-desorption isotherms).

The nitrogen adsorption-desorption isotherms of the AC and MgO-MnO_2-AC are shown in Figure 1(b). According to the International Union of Pure and Applied Chemistry (IUPAC) classification, AC and MgO-MnO_2-AC materials conform to the characteristic of Type I (Sing *et al.* 1985). The Type I isotherm has significant adsorption properties under relatively low pressure and belongs to microporous adsorption. The N_2 isotherm slope of MgO-MnO_2-AC was larger than that of AC, indicating that MgO-MnO_2-AC had higher adsorption performance.

The SEM images of AC and MgO-MnO_2-AC are shown in Figure 2(a) and 2(b). The first image shows the smooth surface with regular pore structure of AC. The latter suggests the surface of AC loaded with MgO and MnO_2 is rough and irregular. Figures 1(a) and 2(b) show that regular holes were destroyed and micropores enlarged. This can be interpreted as the existence of pore expansion in the modification process. Rough surface and macropores improve the adsorption performance of the material. The manganese and magnesium contents of the materials under the best preparation condition are shown in Table 3. The contents of AC loaded with magnesium and manganese were 34.24 and 5.51 $mg \cdot g^{-1}$ respectively. Magnesium and manganese also existed in AC with 16.21 and 0.42 $mg \cdot g^{-1}$. This proved that the loading of manganese and magnesium on AC was successful.

X-ray diffraction patterns of AC and MgO-MnO_2-AC are shown in Figure 3. For the MgO-MnO_2-AC sample, MgO and MnO_2 crystals were found and accounted for the main crystalline part. Both indicated the presence of a crystalline structure evidenced by the appearance of peaks at 29.1°, 44.7° and 58.6° for MnO_2, and 36.9°, 42.7° and 62.3° for MgO. They are in good agreement with the reported Joint Committee on Powder Diffraction Standards (JCPDS) database. It is noted that the sharp peaks corresponding to 21°, 26° and 50° of the original AC disappear, showing that manganese and magnesium interact with AC during the roasting process (Shaabani *et al.* 2015). These characteristic peaks have a certain deviation from the standard diffraction peaks of manganese oxide and magnesium oxide. This shows that manganese oxide, magnesium oxide and AC exist in the form of solid dispersion.

Table 3 | Manganese and magnesium contents of two samples ($mg \cdot g^{-1}$)

Species	Magnesium content	Manganese content
AC	16.21	0.42
MgO-MnO_2-AC	34.24	5.51

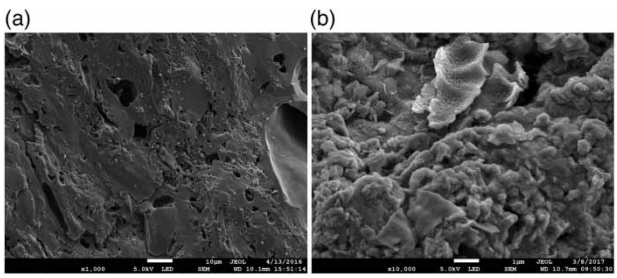

Figure 2 | SEM images of two adsorbents (a: AC, b: MgO-MnO_2-AC).

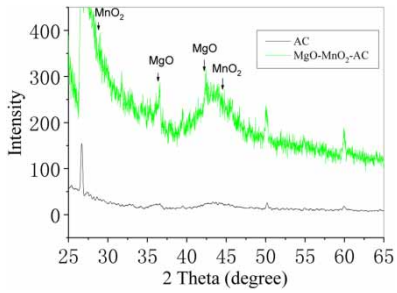

Figure 3 | XRD pattern of AC and MgO-MnO_2-AC.

Adsorption performances of MgO-MnO_2-AC

The adsorption capacity of RB (50 mg·L^{-1}, pH = 7.6) is shown in Figure 4. The experiment was repeated three times. It exhibits that the adsorption rate of MgO-MnO_2-AC to RB was much higher than that of AC, and the adsorption capacity of RB was also significantly higher than that of AC. When adsorption time was 8 h, RB adsorption quantity almost remained stable at 16.0 mg·g^{-1}. The main reason for this phenomenon may be the greater availability of adsorption sites initially, and RB can contact the effective adsorption sites on the MgO-MnO_2-AC rapidly. After the adsorption was completely balanced at about 10 h, the adsorption capacity was 16.19 mg·g^{-1}, 1.68 times that of AC. It may be concluded that MgO-MnO_2-AC has a strong driving force for RB, and the removal rate of MgO-MnO_2-AC after modification is higher.

Effect of dye concentration

The dye concentration has a great impact on the adsorption of RB. The adsorption of RB by AC and MgO-MnO_2-AC increased with the initial concentration of RB (Figure 5). This may be due to active sites on the surface of activated carbon being fully utilized with the increase in RB concentration (Du *et al.* 2017). The adsorption capacity of MgO-MnO_2-AC was significantly higher than that of AC when the dye concentration remained unchanged. On the one hand, MgO-MnO_2-AC increases the specific surface area of activated carbon and the active sites. On the other hand, magnesium oxide and manganese dioxide have synergistic adsorption on dyes at the same time, so under the same conditions, their adsorption capacity increased. We found that when the initial concentration of solution gradually increased, the rate of adsorption increased slowly. This is because when RB concentration was low, there were many active sites of adsorbent and they were not saturated. As the dye concentration increased, more dye molecules

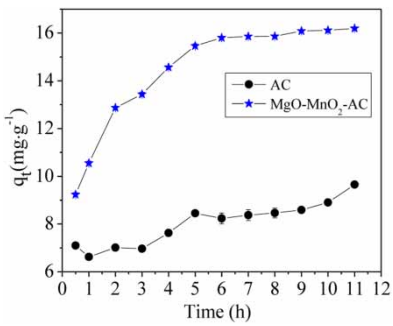

Figure 4 | Effect of time on adsorption capacity for RB.

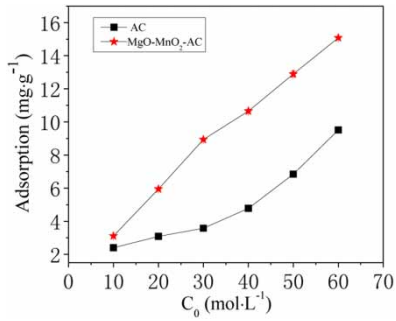

Figure 5 | Effect of RB concentration on the removal capacity.

reduce the number of free adsorption sites, and the adsorption eventually tends to be saturated.

Effect of pH

Experiments investigated the effect of pH on adsorption of RB which is a weakly basic dye. With increasing pH, the adsorption of RB on MgO-MnO_2-AC first increased and then decreased for pH values between 3 and 11 (Figure 6). This is mainly due to the RB molecule containing the Cl^- ion. Under acidic conditions, the adsorbent adsorbs H^+ on the surface and has a positive charge, which causes ion adsorption with the Cl^- ion. With increasing pH, the coexistence of a competitive adsorption with H^+ decreased and RB adsorption increased (Liu *et al.* 2017). Under alkaline conditions, the adsorbent adsorbs hydrated hydroxide ions OH^- and MgO partially hydrolyzed to form OH^-, making the surface of MgO-MnO_2-AC negatively charged, and generating electrostatic repulsion and competition with Cl^- ions in RB, thereby reducing the adsorption value of MgO-MnO_2-AC.

Adsorption kinetics

The adsorption kinetics is one of the most important characters in the whole adsorption process because it can

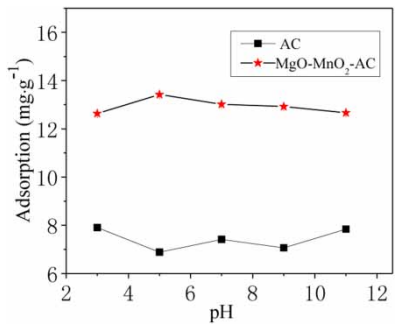

Figure 6 | Effect of pH on the removal of RB by MgO-MnO_2-AC and AC.

demonstrate the solute uptake rate of dyes from aqueous solutions by the adsorbents. In order to investigate the influences of contact time and initial RB concentration on MgO-MnO_2-AC kinetic adsorption, RB initial concentration was in the range between 10 to 100 mg/L, which is presented in Figure 7. The result showed that the equilibration times for adsorption are approximately 8 h at 25 °C with pH of 7.6. From Figure 7, it was observable that the adsorbed amount increased with initial dye concentration. In the kinetic studies, determining the adsorption isotherms, 600 min was allowed to ensure the equilibrium was complete. When reaction time was 600 min, the equilibrium adsorption quantity reached 3.26 $mg{\cdot}g^{-1}$, 16.19 $mg{\cdot}g^{-1}$ and 30.30 $mg{\cdot}g^{-1}$ for 10 $mg{\cdot}L^{-1}$, 50 $mg{\cdot}g^{-1}$ and 100 $mg{\cdot}g^{-1}$ RB, respectively.

In order to analyze the rate controlling of this adsorption process, experimental kinetic data were analyzed according to linear forms of two well-known kinetic models (Mahmoud *et al.* 2013). The pseudo-first-order model and pseudo-second-order model are expressed as follows.

$$\ln(q_e - q_t) = \ln q_e - k_1 t \quad (3)$$

$$\frac{t}{q_t} = \frac{1}{k_2 q_e^2} + \frac{1}{q_e} t \quad (4)$$

where q_e and q_t were the adsorption capacity of dye adsorbed (mg/g) at equilibrium and time t, respectively, and k_1 (min^{-1}) and k_2 ($g{\cdot}mg^{-1}{\cdot}min^{-1}$) are rate constants of pseudo-first-order and pseudo-second-order kinetic models, respectively. Values of k_1, k_2 and R^2 values calculated from the slopes and intercepts are summarized in Table 4. It was clear that the experimental q_e values agreed with the calculated values obtained from the linear plots. The high values of correlation coefficient were 0.9999, 0.9988 and 0.9883 for 10 $mg{\cdot}L^{-1}$, 50 $mg{\cdot}L^{-1}$ and 100 $mg{\cdot}L^{-1}$, respectively. This suggested that the pseudo-second-order equation was adequate to describe the adsorption kinetics of RB on MgO-MnO_2-AC. This model suggests that the adsorption depends on the adsorbent and involves chemisorption and physisorption processes (Kavitha & Namasivayam 2007).

The maximum RB adsorption obtained is 30.30 $mg{\cdot}g^{-1}$ in Figure 7 and, when compared with previously published reports in other studies (Table 5), it suggests that

Table 5 | Comparison of RB adsorption capacity of different adsorbents

Adsorption material	Q_{max} ($mg{\cdot}g^{-1}$)	Reference
AC	9.70	This work
MgO-MnO_2-AC	30.30	This work
Chemically treated *Acacia nilotica* leaves	22.37	Santhi *et al.* (2014)
Heat-activated Sepiolite	8.33	Wang *et al.* (2013)
Rice bran	14.63	Gupta *et al.* (2007)
Cobweb-mediated AgNPs	59.85	Azeez *et al.* (2018)

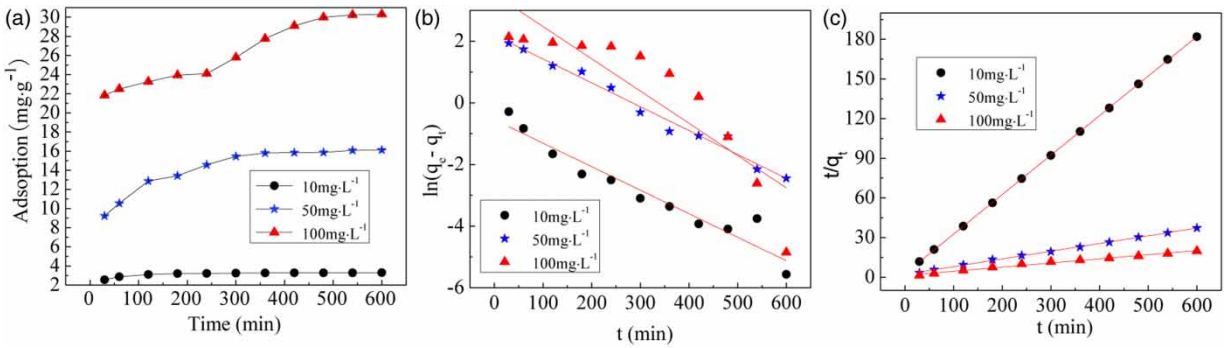

Figure 7 | Adsorption kinetics of RB on MgO-MnO_2-AC. (a) Experimental data, (b) pseudo-first-order, (c) pseudo-second-order.

Table 4 | Fitted kinetic parameter for the adsorption of RB onto MgO-MnO_2-AC

		Pseudo-first-order			Pseudo-second-order		
C_0/$mg{\cdot}L^{-1}$	$q_{e,\ exp}$/$mg{\cdot}g^{-1}$	$q_{e,\ cal}$/$mg{\cdot}g^{-1}$	k_1/min^{-1}	R^2	$q_{e,\ cal}$/$mg{\cdot}g^{-1}$	k_2/$g{\cdot}(mg{\cdot}min)^{-1}$	R^2
10	3.26	0.581	0.0076	0.9242	3.344	0.0330	0.9999
50	16.19	9.012	0.0077	0.9793	17.132	0.0016	0.9988
100	30.30	33.903	0.0105	0.7631	31.959	0.0007	0.9883

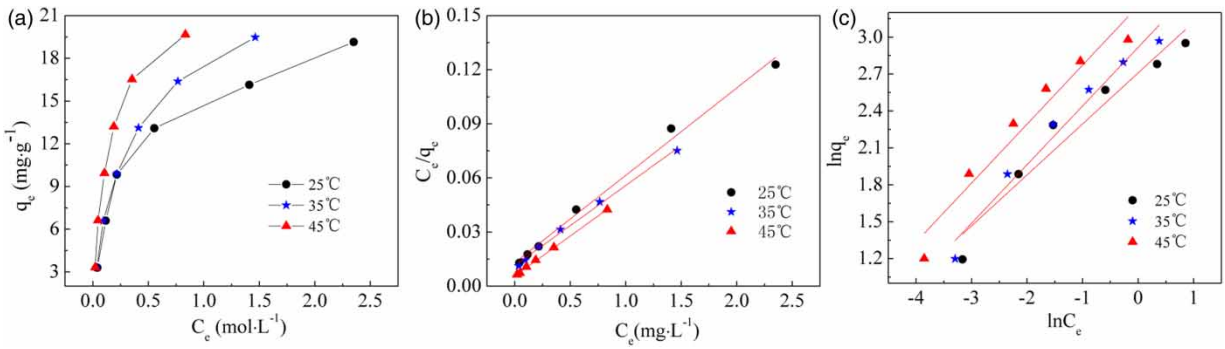

Figure 8 | Adsorption isotherm of RB on MgO-MnO_2-AC. (a) Experimental data, (b) Langmuir, (c) Freundlich.

MgO-MnO_2-AC is a relatively better adsorbent in terms of performance than the adsorbent used before (Gupta *et al.* 2007; Wang. *et al.* 2013; Santhi *et al.* 2014; Azeez *et al.* 2018).

Adsorption isotherms

The adsorption isotherms of MgO-MnO_2-AC are presented in Figure 8. The adsorption of RB by MgO-MnO_2-AC is a nonlinear adsorption process. With the increase of temperature, the equilibrium adsorption capacity of the material at different dye concentrations also increased.

The Langmuir model and Freundlich model were employed to fit the adsorption equilibrium isotherm. The equations were expressed as follows (Yu *et al.* 2009).

Langmuir model:

$$\frac{C_e}{q_e} = \frac{1}{q_m K_L} + \frac{C_e}{q_m} \tag{5}$$

Freundlich model:

$$\ln q_e = \ln K_F + \frac{1}{n} \ln C_e \tag{6}$$

where q_e (mg·g^{-1}) is the adsorption capacity at equilibrium, C_e (mg·L^{-1}) is the concentration of the RB solution at adsorption equilibrium, q_m (mg·g^{-1}) is the maximum adsorption capacity of modified activated carbon, K_L and K_F are constants for adsorption capacity, and n is the constant describing the adsorption strength.

Values of K_L, K_F, R^2 and $1/n$ were calculated and are summarized in Table 6. The correlation coefficients R^2 of the Langmuir isotherm model were all over 0.99. The fitting effect of the Langmuir isotherm model is better than that of the Freundlich isotherm model, and could better describe the adsorption of RB by MgO-MnO_2-AC. It suggested that RB exhibited monolayer adsorption behavior on the MgO-MnO_2-AC surface, which may be caused by electrostatic attraction, hydrogen bond and ion complexation interaction (Çalışkan & Göktürk 2010).

Table 6 | Parameters of Langmuir and Freundlich models for the adsorption of RB on MgO-MnO_2-AC

	Langmuir			Freundlich		
T(°C)	q_m/(mg·g^{-1})	K_L	R^2	1/n	K_F	R^2
25	20.644	3.732	0.9915	0.414	15.005	0.9293
35	22.487	3.928	0.9949	0.477	18.485	0.9631
45	22.573	7.883	0.9992	0.480	25.848	0.9315

CONCLUSIONS

A new type of adsorption material, MgO-MnO_2-AC, was prepared by the impregnation-coprecipitation-calcination method, which made it possible to couple the hydrophilicity of magnesium oxide and manganese dioxide and the high adsorption capacity of activated carbon to greatly improve the pollutant adsorption performance. The content of manganese and magnesium in MgO-MnO_2-AC was 5.51 mg·g^{-1} and 34.24 mg·g^{-1} respectively. The surface area and total pore volume of MgO-MnO_2-AC were all increased to some extent compared to the original activated carbon. The pseudo-second-order adsorption kinetics modeling and Langmuir isotherm can better describe the adsorption of RB on MgO-MnO_2-AC. Internal diffusion process is the rate control step of RB dye adsorption by MgO-MnO_2-AC. The removal of RB on MgO-MnO_2-AC was significantly increased, and the maximum adsorption amount of RB on MgO-MnO_2-AC was 30.30 mg·g^{-1} at 25 °C under

the RB concentration of 100 mg·L^{-1}. The adsorption of RB by AC and MgO-MnO_2-AC increased with the initial concentration of RB. The adsorption of RB first increased and then decreased when pH was between 3 and 11. Based on a favorable removal performance, the modification process was confirmed to be useful and Mn-Mg-GAC can be used as a novel and promising adsorbent material to treat contaminated water with reactive dyes.

ACKNOWLEDGEMENTS

This work is supported by the Open Project of State Key Laboratory of Chemical Engineering (SKL-ChE-13C03) and the Technology Research and Development Program of Tianjin, China (16YFXTSF00390).

REFERENCES

Ahmed, S., Guo, Y., Li, D., Tang, P. & Feng, Y. 2018 Superb removal capacity of hierarchically porous magnesium oxide for phosphate and methyl orange. *Environmental Science and Pollution Research* **25** (25), 24907–24916.

Azeez, L., Lateef, A., Adebisi, S. A. & Oyedeji, A. O. 2018 Novel biosynthesized silver nanoparticles from cobweb as adsorbent for Rhodamine B: equilibrium isotherm, kinetic and thermodynamic studies. *Applied Water Science* **8** (1), 21–32.

Çalışkan, E. & Göktürk, S. 2010 Adsorption characteristics of sulfamethoxazole and metronidazole on activated carbon. *Separation Science and Technology* **45** (2), 244–255.

Cheng, S., Zhang, L., Xia, H., Peng, J., Shu, J. & Li, C. 2016 Ultrasound and microwave-assisted preparation of Fe-activated carbon as an effective low-cost adsorbent for dyes wastewater treatment. *RSC Advances* **6** (82), 78936–78946.

Ciesielczyk, F., Bartczak, P., Zdarta, J. & Jesionowski, T. 2017 Active MgO-SiO_2 hybrid material for organic dye removal: a mechanism and interaction study of the adsorption of C.I. acid blue 29 and C.I. basic blue 9. *Journal of Environmental Management* **204** (1), 123–135.

Du, W., Sun, J., Zan, Y., Zhang, Z., Ji, J., Dou, M. & Wang, F. 2017 Biomass-derived nitrogen-doped hierarchically porous carbon networks as efficient absorbents for phenol removal from wastewater over a wide pH range. *RSC Advances* **7** (74), 46629–46635.

Gupta, V. K., Ali, L. & Saini, V. K. 2007 Adsorption studies on the removal of vertigo blue 49 and orange DNA 13 from aqueous solutions using carbon slurry developed from a waste material. *Journal of Colloid and Interface Science* **315**, 87–93.

Gupta, V. K., Suhas, Tyagi, I., Agarwal, S., Singh, R., Chaudhary, M., Harit, A. & Kushwaha, S. 2016 Column operation studies for the removal of dyes and phenols using a low cost adsorbent. *Global Journal of Environmental Science and Management* **2** (1), 1–10.

Jin, Y., Shen, X., Liu, Z., Wang, Z., Zhu, B., Xu, P., Luo, L. & Zhang, L. 2018 Synthesis of $NiTiO_3$–Bi_2MoO_6 core–shell fiber-shaped heterojunctions as efficient and easily recyclable photocatalysts. *New Journal of Chemistry* **42** (1), 411–419.

Kamran, U., Heo, Y.-J., Lee, J. W. & Park, S.-J. 2019 Chemically modified activated carbon decorated with MnO_2 nanocomposites for improving lithium adsorption and recovery from aqueous media. *Journal of Alloys and Compounds* **794**, 425–434.

Kavitha, D. & Namasivayam, C. 2007 Experimental and kinetic studies on methylene blue adsorption by coir pith carbon. *Bioresource Technology* **98** (1), 14–21.

Li, Q., Tang, X., Sun, Y., Wang, Y., Long, Y., Jiang, J. & Xu, H. 2015 Removal of Rhodamine B from wastewater by modified *Volvariella volvacea*: batch and column study. *RSC Advances* **5** (32), 25337–25347.

Liu, N., Xie, X., Jiang, H., Yang, F., Yu, C. & Liu, J. 2016a Characteristics of estrogenic/antiestrogenic activities during the anoxic/aerobic biotreatment process of simulated textile dyeing wastewater. *RSC Advances* **6** (30), 25624–25632.

Liu, J., He, L., Dong, F. & Hudson-Edwards, K. A. 2016b The role of nano-sized manganese coatings on bone char in removing arsenic(V) from solution: implications for permeable reactive barrier technologies. *Chemosphere* **153**, 146–154.

Liu, Y., Liu, X., Dong, W., Zhang, L., Kong, Q. & Wang, W. 2017 Efficient adsorption of sulfamethazine onto modified activated carbon: a plausible adsorption mechanism. *Scientific Reports* **7** (1), 12437.

Maeda, C. H., Araki, C. A., Moretti, A. L., de Barros, M. A. S. D. & Arroyo, P. A. 2018 Adsorption and desorption cycles of reactive blue BF-5G dye in a bone char fixed-bed column. *Environmental Science and Pollution Research* **26** (28), 28500–28509.

Mahmoud, H. R., El-Molla, S. A. & Saif, M. 2013 Improvement of physicochemical properties of Fe_2O_3/MgO nanomaterials by hydrothermal treatment for dye removal from industrial wastewater. *Powder Technology* **249**, 225–233.

Qi, L. H., Ding, J. D., Ma, X. Q., Guan, X. W., Zhu, W., Yao, H., Zhang, Y. M., Wei, T. B. & Lin, Q. 2019 An azine-containing bispillar arene-based multi-stimuli responsive supramolecular pseudopolyrotaxane gel for effective adsorption of rhodamine B. *Soft Matter* **15** (34), 6836–6841.

Rashidi, R., Moussavi, G., Khavanin, A. & Ghaderpoori, A. 2019 The efficacy of the ozonation process in the presence of activated carbon impregnated with magnesium oxide in the removal of benzene from the air stream. *International Journal of Environmental Science and Technology* **16** (12), 8023–8030.

Riverautrilla, J., Sanchezpolo, M., Gomezserrano, V., Alvarez, P. M., Alvimferraz, M. C. & Dias, J. M. 2017 Activated carbon modifications to enhance its water treatment applications. An overview. *Journal of Hazardous Materials* **187** (1), 1–23.

Rojasmayorga, C. K., Bonillapetriciolet, A., Silvestrealbero, J., Aguayovillarreal, I. A. & Mendozacastillo, D. I. 2015 Physico-chemical characterization of metal-doped bone chars and

their adsorption behavior for water defluoridation. *Applied Surface Science* **355**, 748–760.

Santhi, T., Prasad, A. L. & Manonmani, S. 2014 A comparative study of microwave and chemically treated *Acacia nilotica* leaf as an eco friendly adsorbent for the removal of rhodamine B dye from aqueous solution. *Arabian Journal of Chemistry* **7** (4), 494–503.

Shaabani, A., Hezarkhani, Z. & Badali, E. 2015 Wool supported manganese dioxide nano-scale dispersion: a biopolymer based catalyst for the aerobic oxidation of organic compounds. *RSC Advances* **5** (76), 61759–61767.

Sing, K. S. W., Everett, D. H., Haul, R. A. W., Moscou, L., Pierotti, R. A. & Rouquerol, J. 1985 Reporting physisorption data for gas/solid systems with special reference to the determination of surface area and porosity. *Pure and Applied Chemistry* **57** (4), 603–619.

Song, C., Li, H. & Yu, Y. 2019 Homologous–heterogeneous structure control and intelligent adsorption effect of a polycationic gel for super-efficient purification of dyeing wastewater. *RSC Advances* **9** (17), 9421–9434.

Wang, J., Wang, D., Zhang, G., Guo, Y. & Liu, J. 2013 Adsorption of rhodamine B from aqueous solution onto heat-activated sepiolite. *Wuhan University Journal of Natural Sciences* **18** (3), 219–225.

Wang, K., Zhao, J., Li, H., Zhang, X. & Shi, H. 2016 Removal of cadmium (II) from aqueous solution by granular activated carbon supported magnesium hydroxide. *Journal of the Taiwan Institute of Chemical Engineers* **61**, 287–291.

Xu, P., Shen, X., Luo, L., Shi, Z., Liu, Z., Chen, Z., Zhu, M. & Zhang, L. 2018 Preparation of TiO_2/Bi_2WO_6 nanostructured heterojunctions on carbon fibers as a weaveable visible-light photocatalyst/photoelectrode. *Environmental Science Nano* **5** (2), 327–337.

Yu, J., Li, B. & Sun, X. 2009 Adsorption of methylene blue and rhodamine B on baker's yeast and photocatalytic regeneration of the biosorbent. *Biochemical Engineering Journal* **45** (2), 145–151.

Yuan, P., Liu, D., Tan, D.-Y., Liu, K.-K., Yu, H.-G., Zhong, Y.-H., Yuan, A.-H., Yu, W.-B. & He, H.-P. 2013 Surface silylation of mesoporous/macroporous diatomite (diatomaceous earth) and its function in Cu(II) adsorption: the effects of heating pretreatment. *Microporous and Mesoporous Materials* **170** (170), 9–19.

Zhang, L., Tu, L., Liang, Y., Chen, Q., Li, Z., Li, C., Wang, Z. & Li, W. 2018 Coconut-based activated carbon fibers for efficient adsorption of various organic dyes. *RSC Advances* **8** (74), 42280–42291.

Zhang, H., Hu, J., Xie, J., Wang, S. & Cao, Y. 2019 A solid-state chemical method for synthesizing MgO nanoparticles with superior adsorption properties. *RSC Advances* **9** (4), 2011–2017.

First received 22 December 2019; accepted in revised form 31 March 2020. Available online 22 April 2020